# State Estimation for Linearized MHD Flow

J. Chandrasekar, O. Barrero, A. Ridley, D. S. Bernstein, and B. De Moor

***Abstract*— A state estimation problem for linearized magnetohydrodynamic(MHD) flow is considered. The ideal MHD equations governing the flow of plasma in a three-dimensional channel are linearized about an equilibrium flow. Pseudospectral collocation methods are used to spatially discretize the linear partial differentiation equations and obtain a state-space model of the linearized dynamics. Three different discrete-time Kalman filtering algorithms are used to estimate the state variables, and their performance is analyzed.**

## I. Introduction

Plasma, as a distinct state of matter, plays a crucial role in numerous branches of science and engineering. The Earth is constantly bombarded by low energy plasma emitted by the Sun. However, during flares and coronal mass ejections in the Sun, high energy plasma particles are ejected, causing problems with spacecraft and Earth-based systems [1, 2]. Furthermore, plasma is generated for low-thrust, but highly efficient electric propulsion systems for spacecraft [3, 4]. Finally, plasma confinement and control is one of the main challenges of fusion-based power generation [5]. Plasma flow is the subject of magnetohydrodynamics (MHD), which involves both fluid dynamics and electrodynamics. Consequently, MHD is governed by coupled partial differential equations, which include both the Navier-Stokes equations and Maxwell's equations [6–8].

The present paper is concerned with modeling and state estimation for uncontrolled plasma flows. Our ultimate goal is to apply state estimation techniques to space weather data in order to estimate the state of the plasma flow throughout a region. As a first step in this direction, we linearize the MHD equations for inviscid, incompressible flow in a 3-dimensional channel about a steady flow condition. To spatially discretize these equations, we consider both Fourier and Chebyshev pseudospectral collocation methods [9, 10]. We show that Chebyshev collocation is numerically ill-conditioned for this problem.

Next, we analyze the stability of the truncated linear time-invariant model obtained by the Fourier collocation method. Stability tests show that the resulting model is Lyapunov stable, with all the eigenvalues confined to the imaginary axis. This test is thus inconclusive regarding the stability of the original nonlinear system. The spatially discretized model is then used as the basis for constructing state estimators. We consider the standard Kalman filter in recursive form along with numerically efficient variations, specifically, the reduced rank square root Kalman filter (RRSQRTKF) and the singular square root Kalman filter (SSQRTKF). The use of these filters is motivated by the fact that large-scale MHD models of the magnetosphere typically involve several million states [11].

Application of the Kalman filter shows that observability can be lost due to numerical ill-conditioning corresponding to the clustering of eigenvalues on the unit circle. This fact suggests that a minimum number of measurements may be essential for this class of systems. The presence of eigenvalues on the unit circle also degrades the performance of the RRSQRTKF and SSQRTKF filters, and suggests that numerically efficient filters that are effective for marginally stable systems are needed for MHD.

## II. Ideal MHD Equations

TABLE I
List of symbols

| | |
|---|---|
| $\mu_0$ | permeability of free space (N $A^2$) |
| $\varrho$ | average mass density of plasma (kg/$m^3$) |
| $p$ | pressure (N/$m^2$) |
| $\gamma$ | ratio of specific heats |
| $\vec{u}$ | velocity of the fluid element (m/s) |
| $\vec{J}$ | current density (A/$m^2$) |
| $\vec{E}$ | electric field (Volt/m) |
| $\vec{B}$ | magnetic field (Tesla) |
| $\vec{F}$ | gravity, viscosity, Coriolis forces |

Magnetohydrodynamics (MHD) provides a macroscopic dynamical description of plasma in the presence of electromagnetic fields. The plasma is treated like a fluid with all particles having the same speed. The electromagnetic forces that influence the motion of the particles in the plasma arise from two sources, namely,

This research was supported by the National Science Foundation Information Technology Research initiative, through Grant ATM-0325332.

J. Chandrasekar and D. S. Bernstein are with the Department of Aerospace Engineering, The University of Michigan, Ann Arbor, MI 48109-2140, (734) 764-3719, (734) 763-0578 (FAX), dsbaero@umich.edu

O. Barrero and B. De Moor are with Katholieke Universiteit Leuven, ESAT/SCD-SISTA Department, 3001 Heverlee (Leuven), Belgium.

A. Ridley is with the Department of Atmospheric, Oceanic and Space Sciences, The University of Michigan, Ann Arbor, MI 48109-2143.

internally generated electromagnetic fields (due to the presence and motion of the charged particles in plasma), and externally imposed electromagnetic fields [7].

We assume that the plasma acts as a single fluid, in which the separate identities of positively and negatively charged species are ignored. Furthermore, we assume that the plasma flow occurs in a non-relativistic regime, and we neglect ionization and recombination, which alter the total number of plasma particles. Also, we assume that the conductivity of the plasma is infinite, that is, $\sigma = \infty$. Under these simplifying assumptions the resulting ideal MHD equations are [2, 5, 7]

Mass continuity :

$$\frac{\partial \varrho}{\partial t} + \nabla \cdot (\varrho \vec{u}) = 0, \tag{2.1}$$

Adiabatic equation of state :

$$\frac{d}{dt}\left(\frac{p}{\varrho^{\gamma}}\right) = 0, \tag{2.2}$$

Momentum equation :

$$\varrho \frac{\partial \vec{u}}{\partial t} + \varrho\,(\vec{u} \cdot \nabla)\,\vec{u} = -\nabla p + \vec{J} \times \vec{B} + \vec{F}, \tag{2.3}$$

Ampere's Law (ignoring displacement current):

$$\nabla \times \vec{B} = \mu_0 \vec{J}, \tag{2.4}$$

Faraday's Law :

$$\nabla \times \left(\vec{u} \times \vec{B}\right) = \frac{\partial \vec{B}}{\partial t}, \tag{2.5}$$

Gauss's Law :

$$\nabla \cdot \vec{B} = 0. \tag{2.6}$$

## III. Steady-State Flow and Perturbations in a 3D Channel

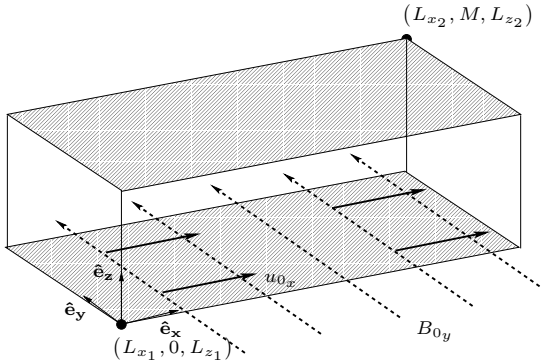



Fig. 1. The plasma is assumed to flow along the $\hat{\mathbf{e}}_{\mathbf{x}}$ direction only. The magnetic field is along $\hat{\mathbf{e}}_{\mathbf{y}}$ and is constant. The magnetic field exerts no pressure on the flow when the velocity of the plasma is parallel to the magnetic field. The pressure exerted by the magnetic field on the plasma when it flows perpendicular to the field depends on the gradient of the magnetic field, which is zero by assumption.

Next, we determine steady-state flow and magnetic field configurations that are consistent with the ideal MHD equations. The domain in this case is the box $\Omega = \{(x, y, z) \in [L_{x_1}, L_{x_2}] \times [0, M] \times [L_{z_1}, L_{z_2}]\}$. Consider a cold plasma (a plasma is cold when the pressure term is negligible in the momentum equation (2.3)), that is, $p \equiv 0$ in (2.3). Furthermore, we assume that the plasma flowing through a 3D channel as shown in Figure 1, is incompressible, which implies that the density is constant, temporally and spatially, that is, $\varrho = \varrho_0$ and hence the adiabatic equation of state (2.2) can be ignored. Let $\vec{u}_0$, $\vec{B}_0$, and $\vec{J}_0$ be the steady state solution of the MHD equations (2.1)-(2.6), that is,

$$\frac{\partial \vec{u}_0}{\partial t} = 0, \quad \frac{\partial \vec{B}_0}{\partial t} = 0, \quad \frac{\partial \vec{J}_0}{\partial t} = 0. \tag{3.1}$$

Hence, it follows from (3.1) and (2.1)-(2.6) that $\vec{u}_0$, $\vec{B}_0$, and $\vec{J}_0$ satisfy

$$\nabla \cdot \vec{u}_0 = 0, \tag{3.2}$$

$$\varrho_0\,(\vec{u}_0 \cdot \nabla)\,\vec{u}_0 = \vec{J}_0 \times \vec{B}_0, \tag{3.3}$$

$$\nabla \times \vec{B}_0 = \mu_0 \vec{J}_0, \tag{3.4}$$

$$\nabla \times \left(\vec{u}_0 \times \vec{B}_0\right) = 0, \tag{3.5}$$

$$\nabla \cdot \vec{B}_0 = 0. \tag{3.6}$$

Note that the gravitational and Coriolis forces have been ignored, that is, $\vec{F} = 0$ in (2.3). Next, assume that the plasma flows along the $\hat{\mathbf{e}}_{\mathbf{x}}$ direction with a constant velocity so that $\vec{u}_0 = u_{0_x}\hat{\mathbf{e}}_{\mathbf{x}}$ and let the constant magnetic field be prescribed by $\vec{B}_0 = B_{0_y}\hat{\mathbf{e}}_{\mathbf{y}}$. Hence, it follows from (2.4) that

$$\vec{J}_0 \quad = J_z(x)\hat{\mathbf{e}}_{\mathbf{z}} = \frac{1}{\mu_0}\frac{\partial B_{0_y}}{\partial x}\hat{\mathbf{e}}_{\mathbf{z}} = 0. \tag{3.7}$$

Substituting (3.7) into (3.3) yields

$$\frac{\partial}{\partial x}\left[\frac{\varrho_0 u_{0_x}^2}{2} + \frac{B_{0_y}^2}{2\mu_0}\right] = 0 \tag{3.8}$$

which is consistent with the assumption that both $\vec{u}_0$ and $\vec{B}_0$ are constant. Note that the prescribed velocity and magnetic field satisfy (3.2) and (3.6), respectively, and hence $\vec{u}_0 = u_{0_x}\hat{\mathbf{e}}_{\mathbf{x}}$ and $\vec{B}_0 = B_{0_y}\hat{\mathbf{e}}_{\mathbf{y}}$ are steady-state solutions of the ideal MHD equations.

Next, define the perturbation variables $\vec{u}_\delta$, $\vec{B}_\delta$ and $\vec{J}_\delta$ by

$$\vec{u}_\delta \triangleq \vec{u} - \vec{u}_0, \quad \vec{B}_\delta \triangleq \vec{B} - \vec{B}_0, \quad \vec{J}_\delta \triangleq \vec{J} - \vec{J}_0. \tag{3.9}$$

Substituting $\varrho = \varrho_0$ and (3.9) into (2.1) yields

$$\frac{\partial \varrho_0}{\partial t} + \varrho_0 \nabla \cdot \vec{u}_0 + \varrho_0 \nabla \cdot \vec{u}_\delta = 0. \tag{3.10}$$

Since the density is constant, substituting (3.2) into (3.10) yields

$$\nabla \cdot \vec{u}_\delta = 0. \tag{3.11}$$

Substituting (3.9) into (2.3), and substituting (3.1) and (3.3) into the resulting equation, and ignoring second and higher order perturbation terms yields

$$\varrho_0 \frac{\partial \vec{u}_\delta}{\partial t} + \varrho_0 \left(\vec{u}_0 \cdot \nabla\right) \vec{u}_\delta + \varrho_0 \left(\vec{u}_\delta \cdot \nabla\right) \vec{v}_0 = \left(\vec{J}_0 \times \vec{B}_\delta\right) + \left(\vec{J}_\delta \times \vec{B}_0\right). \tag{3.12}$$

Substituting (3.9) into (2.4) and using (3.4) yields

$$\nabla \times \vec{B}_\delta = \mu_0 \vec{J}_\delta. \tag{3.13}$$

Substituting (3.9) into (2.5) yields

$$\nabla \times \left[(\vec{u} + \vec{u}_\delta) \times \left(\vec{B} \times \vec{B}_\delta\right)\right] = \frac{\partial}{\partial t}\left(\vec{B}_0 + \vec{B}_\delta\right). \tag{3.14}$$

Substituting (3.1) and (3.5) into (3.14) and ignoring second order perturbation terms yields

$$\nabla \times \left(\vec{v_0} \times \vec{B_\delta}\right) + \nabla \times \left(\vec{v_\delta} \times \vec{B_0}\right) = \frac{\partial \vec{B}_\delta}{\partial t}. \tag{3.15}$$

Substituting (3.9) and (3.6) into (2.6) yields

$$\nabla \cdot \vec{B}_\delta = 0. \tag{3.16}$$

Substituting (3.7), and (3.13) into (3.12) yields

$$\frac{\partial \vec{u}_\delta}{\partial t} + c_1 \frac{\partial \vec{u}_\delta}{\partial x} = c_2 \frac{\partial \vec{B}_\delta}{\partial y} \tag{3.17}$$

and it follows from (3.15) that

$$\frac{\partial \vec{B}_\delta}{\partial t} + c_1 \frac{\partial \vec{B}_\delta}{\partial x} = c_3 \frac{\partial \vec{u}_\delta}{\partial y}, \tag{3.18}$$

where $c_1 \triangleq u_{0_x}$, $c_2 = B_{0_y}/(\varrho_0 \mu_0)$, and $c_3 \triangleq B_{0_y}$. Therefore, (3.11), (3.16), (3.17), and (3.18) are the linearized equations that govern the dynamics of the perturbation variables $\vec{u}_\delta$ and $\vec{B}_\delta$. Note that (3.17) and (3.18) resemble a two-dimensional wave equation.

Taking the partial derivative of (3.17) with respect to $t$ and $x$ yields

$$\partial_{tt} \vec{u}_\delta + c_1 \partial_{tx} \vec{u}_\delta = c_2 \partial_{ty} \vec{B}_\delta \tag{3.19}$$

and

$$\partial_{xt} \vec{u}_\delta + c_1 \partial_{xx} \vec{u}_\delta = c_2 \partial_{xy} \vec{B}_\delta, \tag{3.20}$$

respectively. Taking the partial derivative of (3.18) with respect to $y$ yields

$$\partial_{yt} \vec{B}_\delta + c_1 \partial_{yx} \vec{B}_\delta = c_3 \partial_{yy} \vec{u}_\delta. \tag{3.21}$$

Dividing (3.19) by $c_2$, and multiplying (3.20) by $\frac{c_1}{c_2}$, and adding the resulting equation with (3.21) yields

$$\partial_{tt} \vec{u}_\delta = -2c_1 \partial_{tx} \vec{u}_\delta - c_1^2 \partial_{xx} \vec{u}_\delta + c_2 c_3 \partial_{yy} \vec{u}_\delta. \tag{3.22}$$

Note the symmetry in (3.17) and (3.18) with respect to $\vec{u}_\delta$ and $\vec{B}_\delta$. Hence, a similar procedure yields

$$\partial_{tt} \vec{B}_\delta = -2c_1 \partial_{tx} \vec{B}_\delta - c_1^2 \partial_{xx} \vec{B}_\delta + c_2 c_3 \partial_{yy} \vec{B}_\delta. \tag{3.23}$$

Now, the equations governing the perturbations in the velocity field $\vec{u}_\delta$ and the magnetic field $\vec{B}_\delta$, have been decoupled.

## IV. State-Space Modeling using Spatial Discretization Methods

The partial differentiation equation (3.22) involves the $\partial_{tx}$ operator and hence a separation of variable technique cannot be used to obtain an equivalent ordinary differential equation representation. Hence, we use spatial discretization methods to obtain an ODE model of the linearized perturbation dynamics. Let $\vec{u}_\delta = u_{\delta_x} \hat{\mathbf{e}}_\mathbf{x} + u_{\delta_x} \hat{\mathbf{e}}_\mathbf{y} + u_{\delta_z} \hat{\mathbf{e}}_\mathbf{z}$ and, since (3.22) is a vector equation, we first analyze the solution for $u_{\delta_x}$. Assume $u_{\delta_x}$ has a solution of the form

$$u_{\delta_x} = U_m(x,t) W_m(y), \tag{4.1}$$

where for all $m = 0, 1, \ldots$, $U_m : \mathbb{R} \times \mathbb{R} \to \mathbb{R}$ and $W_m : \mathbb{R} \to \mathbb{R}$. Substituting (4.1) into (3.22) and dividing the resulting equation by $u_{\delta_x}$ yields

$$\frac{\partial_{tt} U_m(x,t)}{U_m(x,t)} + 2c_1 \frac{\partial_{tx} U_m(x,t)}{U_m(x,t)} + c_1^2 \frac{\partial_{xx} U_m(x,t)}{U_m(x,t)} = c_2 c_3 \frac{W_m''(y)}{W_m(y)}, \tag{4.2}$$

which implies that

$$\frac{W_m''(y)}{W_m(y)} = k_m, \tag{4.3}$$

where $k_m \in \mathbb{R}$ is a constant determined by the boundary conditions. We assume that the boundary conditions along $\hat{\mathbf{e}}_\mathbf{y}$ are periodic and given by

$$u_{\delta_x}(x,0,t) = 0, \quad u_{\delta_x}(x,M,t) = 0. \tag{4.4}$$

Note that the no-slip boundary conditions need not be imposed because viscosity has not been included in the ideal MHD equations. It can be shown that the non-trivial solution to (4.3) that satisfies the boundary conditions (4.4) is

$$W_m(y) = w_{0,m} \sin\left(\frac{m\pi y}{M}\right) \tag{4.5}$$

where $w_{0,m}$ is determined by the initial condition and can be assumed to be equal to unity without any loss of generality and

$$k_m = -\omega_{\mathrm{n},m}^2 = -\left(\frac{m\pi}{M}\right)^2. \tag{4.6}$$

Hence, it follows from (4.2) that

$$\partial_{tt} U_m(x,t) + 2c_1 \partial_{tx} U_m(x,t) + c_1^2 \partial_{xx} U_m(x,t) + k_{0,m} U_m(x,t) = 0, \tag{4.7}$$

where $k_{0,m} \in \mathbb{R}$ is defined by

$$k_{0,m} \triangleq c_2 c_3 \omega_{\mathrm{n},m}^2 > 0. \tag{4.8}$$

### A. Fourier Collocation Method

In this section, we assume that the boundary conditions are periodic along the $\hat{\mathbf{e}}_\mathbf{x}$ direction, and hence, express $U_m(x,t)$ as a Fourier series in $x$ with time-varying coefficients. Let $L_{x_1} = 0$ and $L_{x_2} = 2\pi$, and, for $i = 1, \ldots, n$, let $x_{\mathrm{f}i} \triangleq \frac{2\pi(i-1)}{n}$, be the $n$ collocation points along the $\hat{\mathbf{e}}_\mathbf{x}$ direction. Define $q_m^{x_{\mathrm{f}i}}$ by

$$q_m^{x_{\mathrm{f}i}} \triangleq U_m(x_{\mathrm{f}i}, t). \tag{4.9}$$

Next, for all $k = -\frac{n}{2}, \ldots, \frac{n}{2}-1$, define the discrete Fourier coefficients $\tilde{q}_{m_k}$ by

$$\tilde{q}_{m_k} \triangleq \frac{1}{n}\sum_{i=1}^{n} q_m^{x_{\mathrm{f}i}} e^{-\jmath(kx_{\mathrm{f}i})} \tag{4.10}$$

so that $U_m(x,t)$ can be expressed by the discrete Fourier series

$$U_m(x,t) = \sum_{k=-\frac{n}{2}}^{\frac{n}{2}-1} \tilde{q}_{m_k} e^{\jmath(kx)}. \tag{4.11}$$

Next, define $Q_m \in \mathbb{R}^n$ by

$$Q_m \triangleq \begin{bmatrix} q_m^{x_{\mathrm{f}1}} & \cdots & q_m^{x_{\mathrm{f}n}} \end{bmatrix}^{\mathrm{T}}. \tag{4.12}$$

Using the Fourier collocation differentiation matrix [10] in (4.12) yields

$$\ddot{Q}_m + 2c_1\mathcal{D}_{\mathrm{F}n}\dot{Q}_m + c_1^2\mathcal{D}_{\mathrm{F}n}^2 Q_m + k_{0,m}Q_m = 0, \tag{4.13}$$

where $\mathcal{D}_{\mathrm{F}n} \in \mathbb{R}^{n\times n}$ and the $(i,j)$th element of $\mathcal{D}_{\mathrm{F}n}$ is given by

$$\mathcal{D}_{\mathrm{F}n_{(i,j)}} = \begin{cases} \frac{1}{2}(-1)^{i+j}\cot\left[\frac{(i-j)\pi}{n}\right], & i \neq j, \\ 0, & i = j. \end{cases} \tag{4.14}$$

A state-space representation of (4.14) is

$$\begin{bmatrix} \dot{Q}_m \\ \ddot{Q}_m \end{bmatrix} = A_m \begin{bmatrix} Q_m \\ \dot{Q}_m \end{bmatrix}, \tag{4.15}$$

where $A_m \in \mathbb{R}^{2n\times 2n}$ is defined by

$$A_m \triangleq \begin{bmatrix} 0_n & I_n \\ -(c_1^2\mathcal{D}_{\mathrm{F}n}^2 + k_{0,m}I_n) & -2c_1\mathcal{D}_{\mathrm{F}n} \end{bmatrix}. \tag{4.16}$$

Note that $A_m$ can be factored as

$$A_m = P\begin{bmatrix} -c_1\mathcal{D}_{\mathrm{F}n} + \jmath k_{0,m}^{1/2} I_n & 0 \\ S & -c_1\mathcal{D}_{\mathrm{F}n} - \jmath k_{0,m}^{1/2} I_n \end{bmatrix} P^{-1}, \tag{4.17}$$

where $S \in \mathbb{R}^{n\times n}$ is defined by

$$S \triangleq -\left(c_1^2\mathcal{D}_{\mathrm{F}n}^2 + k_{0,m}I_n\right), \tag{4.18}$$

$T \in \mathbb{C}^{n\times n}$ is defined by

$$T \triangleq \left(c_1\mathcal{D}_{\mathrm{F}n} - \jmath k_{0,m}^{1/2} I_n\right) S^{-1}, \tag{4.19}$$

and $P \in \mathbb{R}^{2n\times 2n}$ is defined by

$$P \triangleq \begin{bmatrix} I_n & T \\ 0_n & I_n \end{bmatrix}, \tag{4.20}$$

which implies that

$$\mathrm{spec}(A) = \mathrm{spec}(-c_1\mathcal{D}_{\mathrm{F}n} + \jmath k_{0,m}^{1/2} I_n) \cup \mathrm{spec}(-c_1\mathcal{D}_{\mathrm{F}n} - \jmath k_{0,m}^{1/2} I_n). \tag{4.21}$$

It follows from (4.14) that $\mathcal{D}_{\mathrm{F}n}$ is skew symmetric and hence all its eigenvalues lie on the imaginary axis. Hence, (4.21) implies that the eigenvalues of $A_m$ are also confined to the imaginary axis, that is, for all $\lambda \in \mathrm{spec}(A_m)$, $\mathrm{Re}(\lambda) = 0$. Note that (4.13) is a second order system and can be expressed as

$$M\ddot{Q}_m + G\dot{Q}_m + KQ_m = 0, \tag{4.22}$$

where $M = I_n$, $G = 2c_1\mathcal{D}_{\mathrm{F}n}$, and $K = c_1^2\mathcal{D}_{\mathrm{F}n}^2 + k_0 I_n$. Since $GK = KG$ and $K + \frac{1}{4}GG^{\mathrm{T}}$ is positive definite, it follows from Proposition 3 of [12] that (4.13) is Lyapunov stable.

Note that (4.13) represents the dynamics of the $m$th mode and it follows from the principle of superposition that the solution to (3.22) is given by $u_{\delta_x} = \sum_{m=1}^{\infty} U_m(x,t)W_m(y)$. Retaining $r$ modes and defining the modal state vector $\tilde{Q} \in \mathbb{R}^{2nr}$ by

$$\tilde{Q} \triangleq \begin{bmatrix} Q_1^{\mathrm{T}} & \dot{Q}_1^{\mathrm{T}} & \cdots & Q_r^{\mathrm{T}} & \dot{Q}_r^{\mathrm{T}} \end{bmatrix}^{\mathrm{T}}, \tag{4.23}$$

it follows from (4.15) and (4.16) that

$$\dot{\tilde{Q}} = A\tilde{Q}, \tag{4.24}$$

where $A \in \mathbb{R}^{2nr\times 2nr}$ is the block-diagonal matrix

$$A \triangleq \begin{bmatrix} A_1 & 0 & \cdots \\ 0 & \ddots & 0 \\ \vdots & 0 & A_r \end{bmatrix}. \tag{4.25}$$

Hence,

$$\mathrm{spec}(A) = \mathrm{spec}(A_1) \cup \cdots \cup \mathrm{spec}(A_r) \tag{4.26}$$

and, for all $\lambda \in \mathrm{spec}(A)$, $\mathrm{Re}(\lambda) = 0$.

Let $y_{\mathrm{out},i,j} \triangleq u_{\delta_x}(x_{\mathrm{f}i}, y_j, t)$ be the measured perturbation in the flow velocity $u_x$ from $u_{0_x}$ at $(x_{\mathrm{f}i}, y_j)$, where $x_{\mathrm{f}i}$ is one of the grid points. It follows from (4.1), (4.9), (4.12), and (4.23) that

$$y_{\mathrm{out},i,j} = C_{i,j}\tilde{Q}, \tag{4.27}$$

where $C_{i,j} \in \mathbb{R}^{1\times 2nr}$ has entries

$$C_{i,j} \triangleq \begin{bmatrix} C_{i,j}^1 & \cdots & C_{i,j}^m \end{bmatrix}, \tag{4.28}$$

and, for all $m = 1, \ldots, r$, $C_{i,j}^m \in \mathbb{R}^{2n}$ is defined by

$$C_{i,j}^m = \begin{bmatrix} 0_{i-1} & W_m(y_j) & 0_{2n-i} \end{bmatrix}. \tag{4.29}$$

Next, let $u_{\delta_z} = f(x,y,t)$ so that $\frac{\partial u_{\delta_z}}{\partial z} = 0$. Furthermore, let $u_{\delta_z}$ have a solution of the form (4.9). Note that (3.22) is a vector equation and hence (4.9)-(4.29) will hold with $u_{\delta_x}$ replaced by $u_{\delta_z}$. It then follows from (3.11) that

$$\frac{\partial u_{\delta_x}}{\partial x} = -\frac{\partial u_{\delta_y}}{\partial y}. \tag{4.30}$$

Let $u_{\delta_y}$ have a solution of the form $u_{\delta_y} = \tilde{U}_m(x,t)\tilde{W}_m(y)$ and hence, (4.1) and (4.30) imply that

$$\frac{U_m'(x,t)}{\tilde{U}_m(x,t)} = -\frac{\tilde{W}_m'(y)}{W_m(y)} = \beta_{0,m}, \tag{4.31}$$

where $\beta_{0,m}$ is a constant. Let $\tilde{W}_m(y)$ have a solution of the form

$$\tilde{W}_m(y) = \beta_{1,m}\cos\left(\frac{m\pi y}{M}\right) + \beta_{2,m}, \tag{4.32}$$

where $\beta_{1,m}$ and $\beta_{2,m}$ are determined by the boundary conditions. It then follows from (4.5), (4.30), and (4.31) that $\beta_{0,m} = \beta_{1,m}\frac{m\pi}{M}$.

Next, for all $m = 1, \ldots, r$, define $q_{y,m}^{x_{\mathrm{f}i}} \in \mathbb{R}$ and $Q_{y,m} \in \mathbb{R}^n$ by

$$q_{y,m}^{x_{\mathrm{f}i}} \triangleq \tilde{U}_m(x_{\mathrm{f}i}, t) \tag{4.33}$$

and

$$Q_{y,m} \triangleq \begin{bmatrix} q_{y,m}^{x_{\mathrm{f}1}} & \cdots & q_{y,m}^{x_{\mathrm{f}n}} \end{bmatrix}, \tag{4.34}$$

respectively, where $x_{\mathrm{f}i}$ are the collocation points. Replacing the $\partial_x$ operator in (4.31) with the Fourier collocation differentiation matrix yields

$$Q_{y,m} = \frac{1}{\beta_{0,m}} \mathcal{D}_{\mathrm{F}n} Q_m. \tag{4.35}$$

Define $\tilde{Q}_y \in \mathbb{R}^{2nr \times 2nr}$ by $\tilde{Q}_y \triangleq \begin{bmatrix} Q_{y,1}^{\mathrm{T}} & \dot{Q}_{y,1}^{\mathrm{T}} & \cdots & Q_{y,r}^{\mathrm{T}} & \dot{Q}_{y,r}^{\mathrm{T}} \end{bmatrix}^{\mathrm{T}}$ and hence, it follows from (4.35) that

$$\tilde{Q}_y = \mathcal{T} \tilde{Q}, \tag{4.36}$$

where $\mathcal{T} \in \mathbb{R}^{2nr \times 2nr}$ is defined by

$$\mathcal{T} \triangleq \operatorname{blockdiag}\left(\frac{1}{\beta_{0,1}} \mathcal{D}_{\mathrm{F}n}, \frac{1}{\beta_{0,1}} \mathcal{D}_{\mathrm{F}n}, \cdots, \frac{1}{\beta_{0,r}} \mathcal{D}_{\mathrm{F}n}, \frac{1}{\beta_{0,r}} \mathcal{D}_{\mathrm{F}n}\right) \tag{4.37}$$

Hence, by using a procedure similar to (4.27)-(4.29) the perturbation $u_{\delta_y}(x_{\mathrm{f}i}, y, t)$ can be determined by using (4.36) and the state vector $\tilde{Q}$, whose dynamics are given by (4.24). Note that (3.22) and (3.23) are similar and hence the solution to $\vec{B}_\delta$ is similar to that of $\vec{u}_\delta$, and the constants are determined by the initial and boundary values of the magnetic field instead of the velocity field.

### *B. Chebyshev Collocation Method*

Next, we express $U_m(x, t)$ as a Chebyshev series in $x$ with time varying coefficients. Let $L_1 = -1$ and $L_2 = 1$, and, for all $i = 1, \ldots, n$, let

$$x_{\mathrm{c}i} = -\cos\left[\frac{(i-1)\pi}{n-1}\right] \tag{4.38}$$

be the $n$ Gauss-Lobatto grid points in the interval $[-1, 1]$ (see [9, 10]). Consider a solution of the form (4.1) and define $q_m^{x_{\mathrm{c}i}} \triangleq U_m(x_{\mathrm{c}i}, t)$. The truncated Chebyshev series expansion for the solution $U_m(x, t)$ is (see [9])

$$U_m(x, t) = \sum_{k=0}^{n-1} \tilde{q}_{m_k} \phi_k(x), \tag{4.39}$$

where $\phi_k(x) \triangleq \cos(k \cos^{-1}(x))$, and, for all $k = 0, \ldots, n-1$, $\tilde{q}_{m_k}$ is defined by

$$\tilde{q}_{m_k} \triangleq \frac{1}{\gamma_k} \sum_{i=1}^{n} q_m^{x_{\mathrm{c}i}} \phi_k(x_i) w_i, \tag{4.40}$$

where

$$\gamma_k = \begin{cases} \pi, & k = 0 \text{ or } k = n-1, \\ \frac{\pi}{2}, & 0 < k < n-1, \end{cases} \quad w_i = \begin{cases} \frac{\pi}{2(n-1)}, & i = 1 \text{ or } i = n \\ \frac{\pi}{n-1}, & 1 < i < n. \end{cases} \tag{4.41}$$

Next, defining $Q_m \in \mathbb{R}^n$ by (4.12) with $q_m^{x_{\mathrm{f}i}}$ replaced by $q_m^{x_{\mathrm{c}i}}$ and using the the Chebyshev collocation differentiation matrix (see [10]) in (4.7) yields (4.13) with $\mathcal{D}_{\mathrm{F}n}$ replaced by $\mathcal{D}_{\mathrm{C}n}$, where the $(i, j)$th entry of $\mathcal{D}_{\mathrm{C}n}$ is defined by

$$\mathcal{D}_{\mathrm{C}n_{(i,j)}} = \begin{cases} \frac{c_i}{c_j} \frac{(-1)^{i+j}}{(x_{\mathrm{c}i} - x_{\mathrm{c}i})}, & i \neq j, \\ \frac{-x_{\mathrm{c}i}}{2(1-x_{\mathrm{c}i}^2)}, & 1 < i = j \leq n, \\ \frac{2(n-1)^2+1}{6}, & i = j = 1, \\ -\frac{2(n-1)^2+1}{6}, & i = j = n, \end{cases} \tag{4.42}$$

and $c_i$ is defined by

$$c_i = \begin{cases} 2, & i = 1 \text{ or } i = n, \\ 1, & 1 < i < n. \end{cases} \tag{4.43}$$

The state-space model is then given by (4.24), where $A_m$ is defined by (4.16) with $\mathcal{D}_{\mathrm{F}n}$ replaced by $\mathcal{D}_{\mathrm{C}n}$. The output $y_{\mathrm{out},i,j} \triangleq u_{\delta_x}(x_{\mathrm{c}i}, y_j, t)$ is given by (4.27)-(4.29).

The Chebyshev collocation method is highly sensitive to roundoff when the $\partial_{x^k}$ operator is replaced by differentiation matrix $\mathcal{D}_{\mathrm{C}n}^k$, for $k > 1$. The rate of growth of error is $\mathcal{O}(n^{2k})$ and $\mathcal{O}(n^k)$, for the Chebyshev and Fourier collocation methods, respectively. Certain orthogonal mappings of the Gauss-Lobatto grid points to an alternative set in the interval $[-1, 1]$ can often improve the accuracy of the Chebyshev collocation method. Hence as shown in [13], a new set of grid points can be defined by

$$\tilde{x}_{\mathrm{c}i} = h(x_{\mathrm{c}i}, \alpha) = \frac{\sin^{-1}(\alpha x_{\mathrm{c}i})}{\sin^{-1}(\alpha)}, \tag{4.44}$$

where $x_{\mathrm{c}i}$ is defined in (4.38) and $\alpha \in (0, 1)$. Next, define the diagonal matrix $\mathcal{M}_n \in \mathbb{R}^{n \times n}$ by

$$\mathcal{M}_{n_{(i,j)}} = \begin{cases} 0, \ i \neq j, \\ \frac{1}{h'(x_{\mathrm{c}i}, \alpha)}, \ i = j, \end{cases} \tag{4.45}$$

and define $q_m^{\tilde{x}_{\mathrm{c}i}} \triangleq U_m(\tilde{x}_{\mathrm{c}i}, t)$. Also define $Q_m$ by (4.12) with $q_m^{x_{\mathrm{f}i}}$ replaced by $q_m^{\tilde{x}_{\mathrm{c}i}}$. Using the mapped Chebyshev collocation differentiation matrix in (4.7) yields (4.13) with $\mathcal{D}_{\mathrm{F}n}$ replaced by $\tilde{\mathcal{D}}_{\mathrm{C}n}$, where $\tilde{\mathcal{D}}_{\mathrm{C}n} \triangleq \mathcal{M}_n \mathcal{D}_{\mathrm{C}n}$.

In both cases, namely, the Fourier collocation and mapped Chebyshev collocation, all the eigenvalues of $A$ are confined to the imaginary axis. Due to the roundoff errors in the mapped Chebyshev collocation method, the absolute value of the eigenvalues is very large, which implies that the dynamics as given in (4.24) is oscillatory with very high frequency. Hence, the Fourier collocation method was chosen for simulating the MHD flow. Furthermore, the perturbation $u_{\delta_x}$ at various collocation points is the plant output in all the simulations.

## V. Kalman Filtering Estimator

In this section, three state space observers, namely, the standard Kalman filter (KF) [15], the reduced rank square root filter (RRSQRT) [16], and the singular square root Kalman filter (SSQRTKF) [17], are used to estimate the outputs of the linearized MHD flow system under different measurement noise conditions.

A discrete-time linearized MHD flow model in state space representation is obtained from (4.24) and (4.27) and the dynamics are expressed as,

$$x_{k+1} = A_{\rm d}x_k + w_k \quad (5.1)$$
$$y_k = C_{\rm d}x_k + v_k, \quad (5.2)$$

where $w_k \in \mathbb{R}^{2nr}$ and $v_k \in \mathbb{R}^p$ are uncorrelated process and measurement noise, respectively, and $A_{\rm d}$ and $C_{\rm d}$ are the discrete-time equivalent of $A$ and $C$, respectively. Furthermore, assume that $w_k$ and $v_k$ are white Gaussian noise processes with zero mean and covariance matrices $Q$ and $R$, respectively.

### A. Discrete-Time Kalman Filter

Consider the state observer

$$\hat{x}_{k+1|k} = A_{\rm d}\hat{x}_{k|k-1} + Bu_k + L_k(y_k - C_{\rm d}\hat{x}_{k|k-1}), \quad (5.3)$$

where $L_k \in \mathbb{R}^{n\times m}$ is the Kalman gain and $\hat{x}_{k|k-1}$ is the estimate of $x_k$ based on observations up to time $k-1$. Substituting (5.2) into (5.3) and subtracting (5.1) from the resulting equation yields

$$\tilde{x}_{k+1|k} \triangleq x_{k+1} - \hat{x}_{k+1|k} \quad (5.4)$$
$$= (A_{\rm d} - L_kC_{\rm d})\tilde{x}_{k|k-1} - L_kv_k + w_k, \quad (5.5)$$

where the Kalman gain $L_k$ minimizes the state error covariance matrix $P_{k+1}$ defined by

$$P_{k+1} \triangleq E[(\tilde{x}_{k+1|k} - E[\tilde{x}_{k+1|k}])(\tilde{x}_{k+1|k} - E[\tilde{x}_{k+1|k}])^{\rm T}]. \quad (5.6)$$

The Kalman gain $L_k$ can be obtained by minimizing

$$L_k = \min_{L_k} \alpha^{\rm T}P_{k+1}\alpha. \quad (5.7)$$

As a result, the discrete-time Kalman filter gain is given by

$$L_k = A_{\rm d}P_kC_{\rm d}^{\rm T}(R + C_{\rm d}P_kC_{\rm d}^{\rm T})^{-1}, \quad (5.8)$$

with the error covariance update equation

$$P_{k+1} = A_{\rm d}P_kA_{\rm d}^{\rm T} + Q - A_{\rm d}P_kC_{\rm d}^{\rm T}(R + C_{\rm d}P_kC_{\rm d}^{\rm T})^{-1}C_{\rm d}P_kA_{\rm d}^{\rm T}, \quad (5.9)$$

which is a discrete Riccati difference equation (DRDE). If the system is observable and $k \to \infty$, $P_k$ converges to a steady-state positive semidefinite matrix $P$, and $L_k$ approaches the constant matrix $L$, given by

$$L = A_{\rm d}PC_{\rm d}^{\rm T}(R + C_{\rm d}PC_{\rm d}^{\rm T})^{-1}, \quad (5.10)$$

where $P$ satisfies the discrete algebraic Riccati equation (DARE)

$$P = A_{\rm d}PA_{\rm d}^{\rm T} + Q - A_{\rm d}PC_{\rm d}^{\rm T}(R + C_{\rm d}PC_{\rm d}^{\rm T})^{-1}C_{\rm d}PA_{\rm d}^{\rm T}. \quad (5.11)$$

Alternatively, Kalman and Bucy [18] showed that a recursive estimate update is optimal for several criteria, such as minimum variance and maximum likelihood. For the estimate of $x_{k+1}$ given $Y_k = \{y_l,\ l = 0, \ldots, k\}$ denoted by $\hat{x}_{k+1|k}$, the Kalman filter equations are given by

$$P_{k|k} = A_{\rm d}P_{k|k-1}A_{\rm d}^{\rm T} + Q, \quad (5.12)$$
$$L_k = P_{k|k}C_{\rm d}^{\rm T}(C_{\rm d}P_{k|k}C_{\rm d}^{T} + R)^{-1}, \quad (5.13)$$
$$P_{k+1|k} = P_{k|k} - L_kC_{\rm d}P_{k|k}, \quad (5.14)$$
$$\hat{x}_{k|k} = A_{\rm d}\hat{x}_{k|k-1} + Bu_k, \quad (5.15)$$
$$\hat{x}_{k+1|k} = \hat{x}_{k|k} + L_k(y_k - C_{\rm d}x_{k|k-1}). \quad (5.16)$$

Since the Kalman Filter is prohibitive for large scale systems, we consider suboptimal Kalman filters, namely, RRSQRT, and SSQRTKF.

### B. SSQRTKF Algorithm

SSQRTKF is based on (5.9) assuming $Q = 0$, which implies that the variance of the process noise is zero. By definition, the Schur complement of (5.9) with $Q = 0$ is the matrix,

$$M = \begin{pmatrix} R + C_{\rm d}P_kC_{\rm d}^{\rm T} & C_{\rm d}P_kA_{\rm d}^{\rm T} \\ A_{\rm d}P_kC_{\rm d}^{\rm T} & A_{\rm d}P_kA_{\rm d}^{\rm T} \end{pmatrix}, \quad (5.17)$$

with $R \triangleq L_RL_R^{\rm T}$ and $P_k \triangleq S_kS_k^{\rm T}$. A QR decomposition of $M$ yields

$$\begin{pmatrix} L_R & C_{\rm d}S_k \\ 0 & A_{\rm d}S_k \end{pmatrix} U_k = \begin{pmatrix} \hat{F}_k & 0 \\ \hat{K}_k & S_{k+1} \end{pmatrix}, \quad (5.18)$$

where $U_k$ is orthogonal and $S_k$ is $n\times l$, with $l$ chosen larger than the number of unstable eigenvalues of $A_{\rm d}$. Note that the QR decomposition is computed for a small matrix of size $(p+l)\times p$ making it cheap to compute. Alternatively, the Kalman filter gain can be computed from $\hat{F}_k$ and $\hat{K}_k$ by $L_k = \hat{K}_k\hat{F}_k^{-1}$, assuming $F_k$ is invertible. Since $F_k$ is diagonally dominant as a result of the QR decomposition, instead of computing $F_k^{-1}$, we invert its diagonal entries to obtain a diagonal approximation of $F_k^{-1}$. Moreover, if $A_{\rm d}$ and $C_{\rm d}$ are sparse, the construction of the left factor in the left hand side of (5.18) is cheap as well.

A key characteristic of the SSQRTKF algorithm is that the spectrum of the state space observer dynamics matrix $A_{\rm d} - L_kC_{\rm d}$ is constructed by reflecting the eigenvalues of $A_{\rm d}$ with $|\lambda| > 1$ to their unit circle mirror images $1/|\lambda|$, and leaving the eigenvalues with $|\lambda| < 1$ unchanged.

### C. RRSQRT Algorithm

In the RRSQRT algorithm the square root factors are based on an eigendecomposition. Let $P_{k|k} = V_k\Lambda_kV_k^{\rm T}$ be the eigendecomposition of the error covariance matrix $P_{k|k}$, so that $S_{k|k} = V_k\Lambda_k^{1/2}$ is a square root factor of $P_{k|k}$. The error covariance matrix is now approximated by using only $q$ leading eigenvalues. With the ordering $|\lambda_1| \geq \ldots \geq |\lambda_n| \geq 0$, an approximation is obtained by truncating $S_{k|k}$ after the first $q$ columns. The three main steps are the time step, the reduction step, and the measurement step.

**a. Time step:** The time step performs the time propagation of the state estimate and error covariance and are equivalent to the Kalman filter equations, which implies that

$$\begin{aligned} \hat{x}_{k+1|k} &= A_{\mathrm{d}}\hat{x}_{k|k-1} + Bu_k + L_k(y_k - \hat{y}_{k|k}) \\ S_{k|k} &= [AS_{k|k-1}\ BQ^{1/2}], \end{aligned} \tag{5.19}$$

where $S_{k|k}$ is the $n \times q$ estimate square root of the error covariance $P_{k|k}$.

**b. Reduction step:** The addition of rows, $BQ^{1/2}$ in equation (5.19), for the system noise in every time step quickly increases the computation time. Therefore the number of columns is reduced to $q$ after every time-step. The idea for this approximation is to use only the first $q$ leading eigenvalues and eigenvectors of the error covariance matrix $S_{k|k}S_{k|k}^T$. For efficient implementation, the eigendecomposition of the matrix $S_{k|k}^{\mathrm{T}}S_{k|k}$ is determined by $S_{k|k}^{\mathrm{T}}S_{k|k} = V_k\Lambda_k V_k^{\mathrm{T}}$. It can be shown that

$$(S_{k|k}V_k\Lambda_k^{-1/2})\Lambda_k(S_{k|k}V_k\Lambda_k^{-1/2})^{\mathrm{T}} = S_{k|k}S_{k|k}^{\mathrm{T}} \tag{5.20}$$

and thus, $S_{k|k}^* = [S_{k|k}V_k]_{1:n,1:q}$ is the square root of the optimal rank $q$ approximation of $S_{k|k}S_{k|k}^{\mathrm{T}}$.

The above procedure is much faster than eigenvalue computations on the matrix $S_{k|k}S_{k|k}^{\mathrm{T}}$ or singular value computations on $S_{k|k}$, which could also accomplish the task of reduction. The speed up is due to the fact that the matrix $S_{k|k}^{\mathrm{T}}S_{k|k}$ is a $q+m \times q+m$ matrix and $q, m \ll n$.

**c. Measurement step:** The measurements update for scalar measurements $p = 1$ is given by

$$\begin{aligned} &H_k = S_{k|k}^{*\mathrm{T}}C_{\mathrm{d}}^{\mathrm{T}}, \gamma_k = (H_k^{\mathrm{T}}H_k + R)^{-1}, \\ &L_{k+1} = S_{k|k}^* H_k\gamma_k, S_{k+1|k} = S_{k|k}^* - L_{k+1}H_k^{\mathrm{T}}[1 + (\gamma_k R)^{1/2}]^{-1}, \end{aligned} \tag{5.21}$$

with $L_{k+1}$ the suboptimal Kalman filter gain. If there are multiple measurements, these can be processed sequentially. The number of computations required in the time propagation of the error in the covariance, which is a major fraction of the total number, is reduced by a factor $n/q$ with respect to the original Kalman filter algorithm. It can be shown that for $q = n$ the RRSQRT algorithm is exact in the sense that it is equivalent to the Kalman filter equations. The parameter $q$ controls the accuracy of the approximation. The price for greater accuracy is a larger computational burden. Table II shows a comparison of the computation complexity of the three methods introduced above. In the first row, the number of flops needed for one iteration is shown . In the second row, the number of flops needed for one iterations when $n \gg, m, l, q, p$, is shown.

TABLE II

COMPARISON OF THE COMPUTATION COMPLEXITY BETWEEN KALMAN FILTER, RRSQR FILTER, AND SSQRTKF ALGORITHM.

| | Kalman Filter | SSQRTKF | RRSQRT |
|---|---|---|---|
| flops | $2n(3n^2 + 4mn + n/2 + m^2) + 2m(m^2/3 + 1)$ | $2n(nl + 2m^2 + 3ml + l^2) + 2m[(l - 2/3m) + 1/2]$ | $2n[p^2 + 2q^2 + (2m + n)q] + 3q(4q^2 + m)$ |
| $\sim$ flops $n \gg m, l, q, p$ | $2n^2l$ | $6n^3 + (8m + 1)n^2$ | $2n^2q$ |

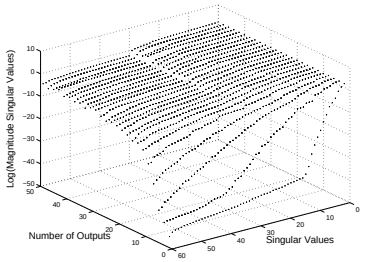



Fig. 2. Logarithm of the singular values of the observability matrix for different number of measurements. We observe that the condition number of the observability matrix is high for a small number of measurements and the condition number is small when the number of measurements is larger than $\sim 9$ .

## VI. STATE ESTIMATION FOR THE LINEARIZED MHD MODEL

We consider a $10 \times 10$ grid with equidistant points (the grid points along the $\hat{\mathbf{e}}_{\mathbf{x}}$ direction are the Fourier collocation points), where $0 < x < 2\pi$, $0 < y < 1$, and sample time $T_s = 10^{-3}$ seconds. The number of modes retained is $m = 3$ and hence, $A_{\mathrm{d}} \in \mathbb{R}^{60\times 60}$, and $C_{\mathrm{d}} \in \mathbb{R}^{100\times 60}$. Although the system may be fully observable with just one measurement output, the discrete-time linearized system turns out to be marginally observable, because all the poles are clustered on the unit circle, which entails numerical round-off error.

It can be see from Figure 2 that at least 9 measurements are needed to guarantee the full observability of the system. On the other hand, since the system is marginally observable all the modes of the system are needed to obtain a reliable estimator as shown in Figure 3. Figure 4 shows that Kalman and RRSQRT filters behave in a similar manner, while the performance of SSQRTKF is poor. In the same plot, since the system is marginally observable, we observe that by increasing the measurement noise, SSQRTKF becomes unstable, whereas, KF and RRSQRT become noisy. The plot on the left in Figure 5 shows a reduction in the RMSE and the oscillations, when the number of measurements is increased to 31, and the same measurement noise condition as in Figure 4 with

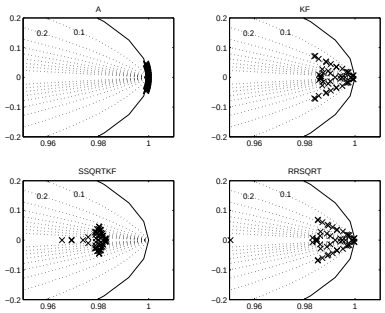



Fig. 3. Eigenvalues of the discrete model and the three observers. For the three methods we have chosen 18 output measurements. For RRSQRT $q = 60$, and for SSQRTKF $l = 60$. As expected, we observe that the location of the eigenvalues for the Kalman and RRSQRT filters are very similar. The number of iterations required for RRSQRT and SSQRTKF to converge to this solution was 800 and 500, respectively.

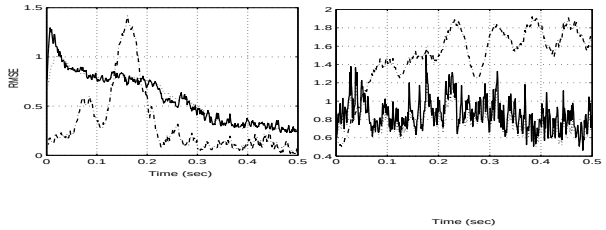



Fig. 4. RMSE of the estimated outputs taking 18 measurements. Solid line KF, dash-dot line SSQRTKF, and dotted line RRSQRT. On the left, a signal-to-noise ratio $\mathrm{SNR} = 18$dB for the measurement noise, and no process noise was used. On the right, a $\mathrm{SNR} = 4$dB for the measurement noise, and no process noise was used. The RMSE magnitude of SSQRTKF on the left has been scaled by 0.1.

$\mathrm{SNR} = 4$dB is used. The plot on the right shows the RMSE with $\mathrm{SNR} = -9.5$dB in which case the system becomes noisy but RMSE is low.

## VII. Conclusion

A discrete-time linearized model for the flow of plasma in a three-dimensional channel was obtained. The obtained model is marginally stable and has oscillatory dynamics which makes the system difficult to observe. Three different state space observers were studied, namely, Kalman filter, RRSQRT filter, and SSQRTKF filter.

The Kalman filter performs well, and is very reliable and robust as shown in Figures 4, and 5. The drawback of the Kalman filter is that it is prohibitive to compute for large scale systems. On the other hand, RRSQRT and SSQRTKF exhibit numerical problems because all the eigenvalues of $A_{\mathrm{d}}$ have to be included to design a stable observer. Moreover, these methods are based on the square root algorithm, and hence their convergence rate is low when the eigenvalues of $A_{\mathrm{d}}$ are located very close to the unit circle. As mentioned in figure (3) the number of iteration for RRSQRT, and SSQRTKF are

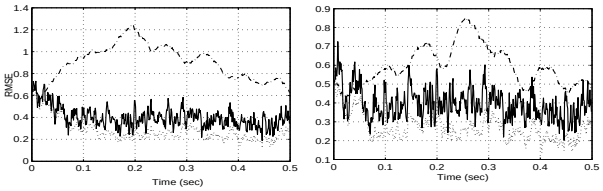



Fig. 5. RMSE of the estimated outputs taking 31 measurements. Solid line Kalman filter, dash-dot line SSQRTKF, and dotted line RRSQRT. On the left, no process noise, and measurements noise with $\mathrm{SNR} = 4$dB was used. On the right, no process noise and measurement noise with $\mathrm{SNR} = -9.5$dB was used.

very high. Therefore, we cannot exploit the advantages of the proposed suboptimal Kalman filters for the linearized MHD model.

## References

[1] I. A. Daglis, *Space Storms and Space Weather Hazards*, Kluwer Academic Publishers, 2001.
[2] M. B. Kallenrode, *Space Physics*, Springer, 2000.
[3] W. R. Corliss, *Propulsion Systems for Space Flight*, McGraw-Hill Book Company, 1960.
[4] P. Y. Peterson, A. D. Gallimore, and J. M. Haas, "An experimental investigation of the internal magnetic field topography of an operating Hall thruster," *Physics of Plasmas*, vol. 9, pp. 4354-4362, 2002.
[5] J. P. Freidberg, *Ideal Magnetohydrodynamics*, Plenum Press, 1987.
[6] R. O. Dendy, *Plasma Physics - An Introductory Course*, Cambridge University Press, 1993.
[7] Tamas. I. Gombosi, *Physics of the Space Environment*, Cambridge University Press, 1998.
[8] P. C. Kendall and C. Plumpton, *Magnetohydrodynamics with hydrodynamics*, Pergamon Press, 1964.
[9] O. M. Aamo and M. Kristic, *Flow Control by Feedback - Stabilization and Mixing*, Springer, 2003.
[10] C. Canuto, M. Y. Hussaini, A. Quarteroni, and T. A. Zang, *Spectral Methods in Fluid Dynamics*, Springer-Verlag, 1988.
[11] C. P. T. Groth, D. L. D. Zeeuw, T. I. Gombosi, and K. G. Powell, "Global three-dimensional MHD simulation of a space weather event: CME formation, interplanetary propagation, and interaction with the magnetosphere," *J. Geo. Phy. Res.*, vol. 105, pp. 25,053-25,078, 2000.
[12] D. S. Bernstein and S. P. Bhat, "Lyapunov Stability, Semistability and Asymptotic Stability of Matrix Second Order Systems," *Trans. of ASME.*, 50th Anniversary Design Issue, pp. 145-153, 1995.
[13] W. S. Don and A. Solomonoff, "Accuracy Enhancement for Higher Derivatives using Chebyshev Collocation and a Mapping Technique," *SIAM J. Sci. Comp.*, vol. 18, pp. 1040-1055, 1997.
[14] M. Morf and T. Kailath, "Square-Root Algorithms for Least-Squares Estimation," *IEEE Trans. Auto. Contr*, vol. 20, pp. 487-497, 1975.
[15] R. E. Kalman, "A New Approach to Linear Filter and Prediction Theory," *J. Basic. Engr.*, vol. 82D, pp. 35-45, 1960.
[16] M. Verlaan and A. W. Heemink, "Reduced Rank Square Root Filters for Large Scale Data Assimilation Problems," *2nd Int. Symp. on Assimilation of Observations in Meteorology and Oceanography, World Meteorological Organization*, pp. 247-252, 1995.
[17] O. Barrero and B. De Moor, "A Singular Square Root Algorithm for Large Scale Systems," *Proc. 15th IASTED Int. Conf. Model. Sim., Marina del Rey, USA*, March 2004.
[18] R. Kalman and R. Bucy, "New Results in Linear Filtering and Prediction Theory," *J. Basic. Engr*, vol. 83D, pp. 95-108, 1961.